Supplemental Table 1 MSN synthesis materials.

| Chemicals and supplies	Source	Source Location
DOTA-NHS ester	Macrocyclics, Inc.	Dallas, TX, USA
Tetraethyl orthosilicate (TEOS)	Sigma-Aldrich Co. LLC.	St. Louis, MO, USA
Ammonium hydride	Sigma-Aldrich Co. LLC.	St. Louis, MO, USA
Hexadecyl trimethyl ammonium bromide (CTAB)	Sigma-Aldrich Co. LLC.	St. Louis, MO, USA
3-aminopropyl triethoxysilane (APS)	Sigma-Aldrich Co. LLC.	St. Louis, MO, USA
Ammonium acetate	Sigma-Aldrich Co. LLC.	St. Louis, MO, USA
PD-10 columns	GE Healthcare	Piscataway, NJ, USA
Absolute ethanol	Fisher Scientific	Pittsburg, PA, USA
MES buffer	Fisher Scientific	Pittsburg, PA, USA
Dimethyl sulfoxide (DMSO)	Fisher Scientific	Pittsburg, PA, USA

Supplemental Table 2 Synthesis of MSN.
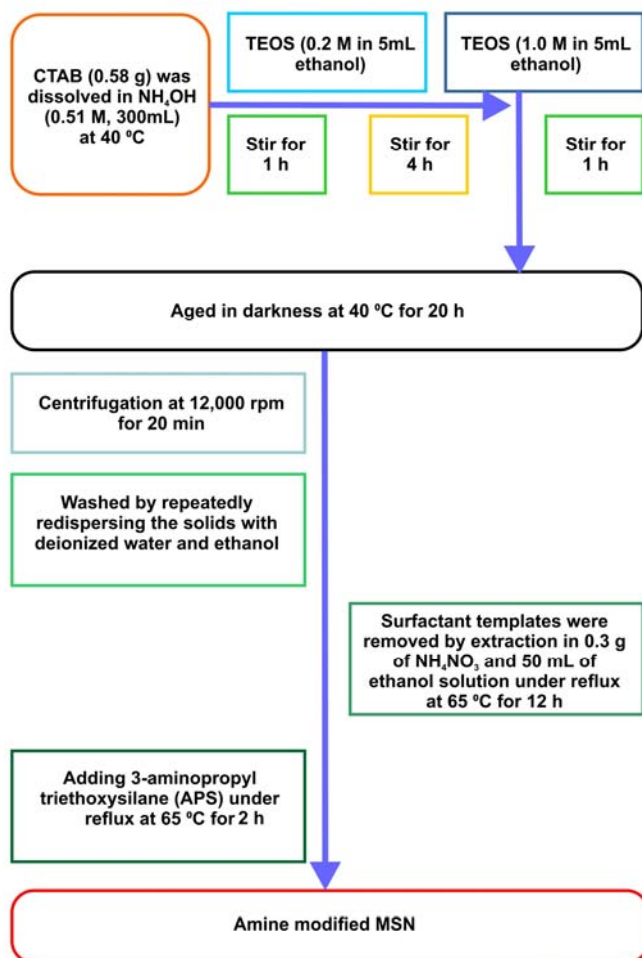
In order to synthesize MSN, the sol-gel co-condensation of TEOS was performed as follows. CTAB (0.58 g) was dissolved in NH$_4$OH (0.51 M, 300 mL) at 40 °C. After stirring for 1 hour, TEOS (0.2 M in 5 mL ethanol) was added and the solution was stirred for an additional 4 hours. Thereafter, a high concentration of TEOS (1.0 M in 5.0 mL of ethanol) was added under vigorous stirring for an additional hour. The solution was aged in darkness at 40 °C for 20 hours. Samples were subsequently collected by centrifugation at 12,000 rpm for 20 minutes, and then washed by repeatedly re-dispersing the solids with deionized water and ethanol. Surfactant templates were removed by extraction in 0.3 g of NH$_4$NO$_3$ and 50 mL of ethanol solution under reflux at 65° C for 12 hours. The amine modified MSN were post-synthesized by adding 3-aminopropyl triethoxysilane (APS) under reflux at 65° C for 2 hours. The samples were collected and washed as described above.

Supplemental Table 3. Characterization of physical properties of MSN

Samples	S_{BET}[a] (m^2/g)	W_{BJH}[a] (nm)	Zeta potential ζ[b] (mV)	Particle size via DLS[b] (nm)
MSN-NH$_2$	698	3.9	$+$22±4.9	123.7±23.5
MSN-DOTA	588	3.8	$+$36.5±7.9	125.6±17.5
MSN-DOTA-^{111}In	505	3.5	$+$10.8±5.4	125.8±18.8

[a] Nitrogen adsorption–desorption measurements were made on a Micromertics ASAP 2020 at 77 K. Surface area and pore size determinations were obtained using Brunauer–Emmett–Teller (BET) and Barrett–Joyner–Halenda (BJH) methods, respectively.

[b] ζ potential and hydrodynamic radius of MSN (suspended in DI, pH 7.4) were obtained via a Malvern Zetasizer.
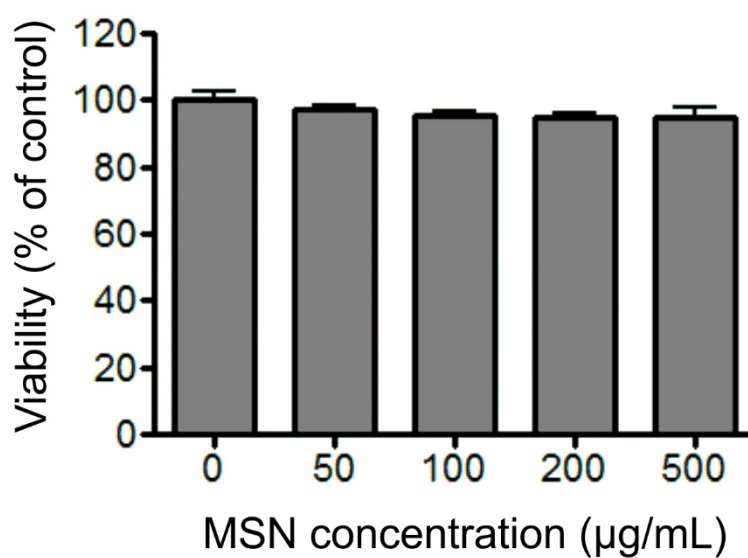
Supplemental Figure 1. Effect of MSN on viability of NSCs. NCSs were loaded with various concentrations of MSN for 2 hours in Opti-MEM medium, after which medium was replaced with DMEM containing 10% FBS. The viability of cells was measured 24 hours later using standard MTT assay (Roche Diagnostics, Mannheim, Germany).
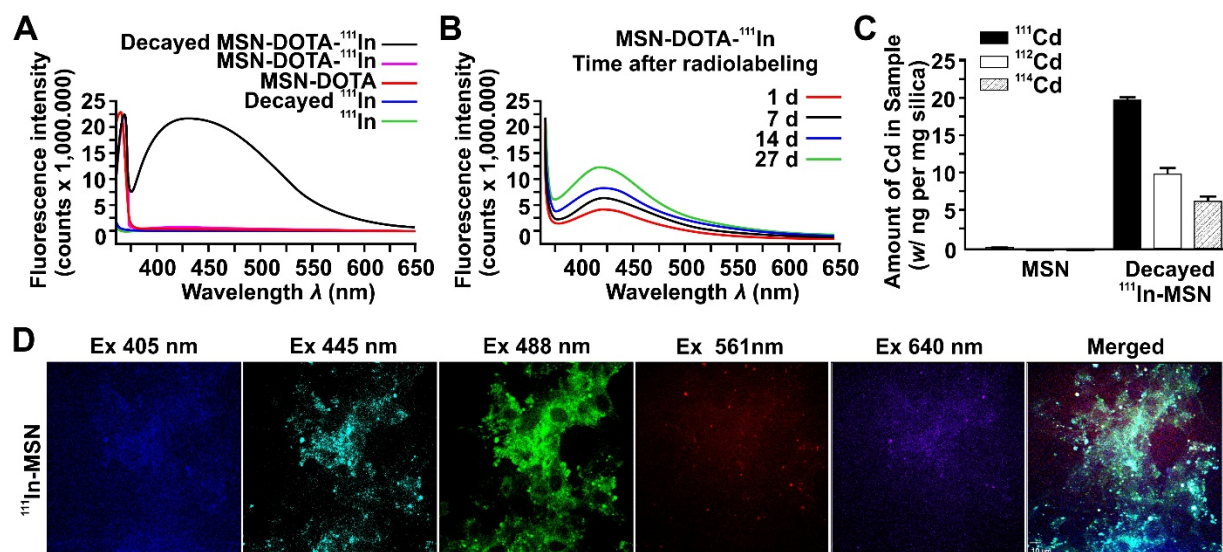
Supplemental Figure 2. Fluorescence emission of ^{111}In-MSN was formed during the decay process. A. Fluorescence spectra of active and decayed ^{111}In or ^{111}In-MSN were measured using HORIBA Fluorolog-3 Spectrofluorometer (HORIBA Instruments, Inc., New York, NY). All samples were excited at 350 nm with 14mm slit and all measurements were performed in water at room temperature. B. Time course of the observed increase in acquisition of the spectra properties. C. Quantification of Si and Cd was accomplished using ICP-MS as described in the Material and Methods. Amount of Cd in the sample was normalized per weight of Si. No isotopes of Cd were detected in control MSN, whereas fully decayed ^{111}In-MSN contained preferentially ^{111}Cd isotope, and in lesser amounts, isotopes of ^{112}Cd and ^{114}Cd. D. To characterize the fluorescent profiles of NSCs loaded with decayed ^{111}In-MSN, confocal images using 5 separate color channels, excited by lasers with 405nm (blue), 445nm (cyan), 488nm (green), 561nm (red), 640nm (far red) wavelengths, were collected. The green channel showed the strongest fluorescence signal.

After the fluorescent spectra of active and decayed ^{111}In in solution as well as in as ^{111}In-MSN complex were compared, it is confirmed that the fully decayed ^{111}In-MSN sample showed wide fluorescent spectra ranging from 350nm to 650nm (peak at 425 nm). In contrast, no fluorescence was observed in MSN-DOTA alone, active ^{111}In-MSN, and active or decayed free

[111]In samples (Supplemental Fig. 2A). Moreover, fluorescence emission of ^{111}In-MSN complex was formed during the decay process (Supplemental Fig. 2B). The wide fluorescent spectra of our decayed ^{111}In-MSN suggest that observed phenomenon is most likely due to the size of MSN and weakly coordinated Cd inside of MSN. [111]In is known to decay to [111]Cd(*1*). Indeed, the ICP-MS analysis of fully decayed ^{111}In-MSN complex revealed the presence of [111]Cd at the level of 19.7±0.4 ng per mg of Si. Isotopes of [112]Cd (9.7±0.8 ng per mg of Si) and [114]Cd (6.2±0.7 ng per mg of Si) were also detected, but no Cd isotopes were detected in control MSN-DOTA samples (Supplemental Fig. 2C). In support of our observations, Bruchez et al., reported that CdSe nanocrystals emit fluorescence in green-yellow-red range in size-dependent (2.4-4.6 nm) fashion(*2*). Sooklal et al. demonstrated that CdS/dendrimer nanocomposites generate a wide spectrum with emission maxima at about 450 nm upon excitation at a wavelength of 340 nm. Authors also observed that emission spectra is more complex for CdS/dendrimer nanocomposites prepared in water due to the presence of larger CdS clusters than in methanol preparation(*3*). The complex nature of fluorescent spectra of our decayed ^{111}In-MSN warrants further   investigations.
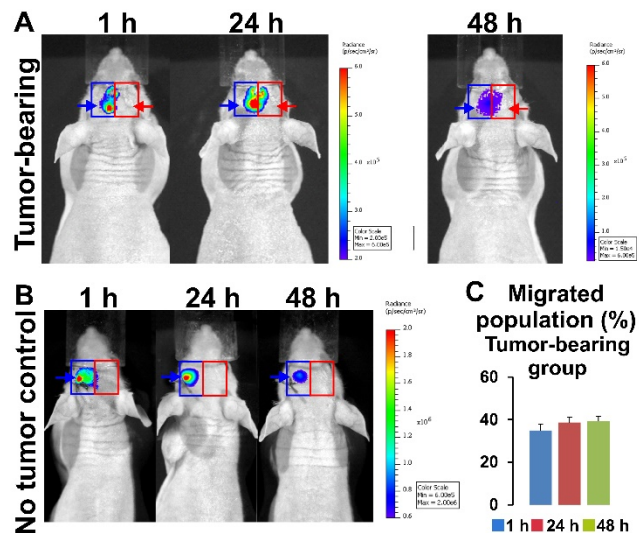
Supplemental Figure 3. Bioluminescence imaging of the mouse brain after intracerebral delivery of ^{111}In-MSN-loaded NSCs. A. Distribution of NSCs in tumor-bearing animals (n=4) at 1, 24 and 48 hours after injection. Image of representative animal is shown. Injection sites for NSCs and glioma cells are indicated by blue and red arrows respectively. B. Localization of NSCs in the control, non-tumor bearing animals (n=4) at 1, 24 and 48 hours after injection. C. Migrated populations of NSCs in tumor-bearing animals were calculated by drawing the region of interest (ROI) corresponding to the left (blue square) and right (red square) sides of the brain and measuring of the normalized luminescent signal within ROI for each assessed time point. ***$p<0.001$, repeated measures ANOVA with Bonferroni's post hoc test.

BLI of control and tumor-bearing mice implanted with radiolabeled NSCs was performed at 1, 24 and 48 hours post-surgery. In the tumor-bearing animals, the migration of a small fraction of NSCs away from the NSCs injection site was observed within 1 hour post-implantation (33±3% of total luminescence) with a sustained migration pattern towards the right hemisphere at 24 (33.5±3.5% of total luminescence) and 48 hours (37.7±5% of total

luminescence, n=4, *p<0.001*; Supplemental Fig. 3A). Supplemental Fig. 3B shows that NSCs loaded with radiolabeled MSN are localized at the injection site in the control (non-tumor-bearing animal, n=4) at 1, 24 and 48 hours, respectively. It is important to note that, while we were able to distinguish non-migratory and migratory patterns of NSCs behavior in control and tumor-bearing animals respectively by BLI, this method does not allow us to precisely quantify the fraction of migrated NSCs due to the measuring of surface radiance and lack of precise spatial information. Thus, our data demonstrates that NSCs localized at the injection site in control animals, but migrated and reached the tumor engraftment site in tumor-bearing animals as shown by SPECT with further confirmation by BLI, which is in agreement with our knowledge of NSC behavior in naïve and tumor-bearing animals(*4,5,6*).
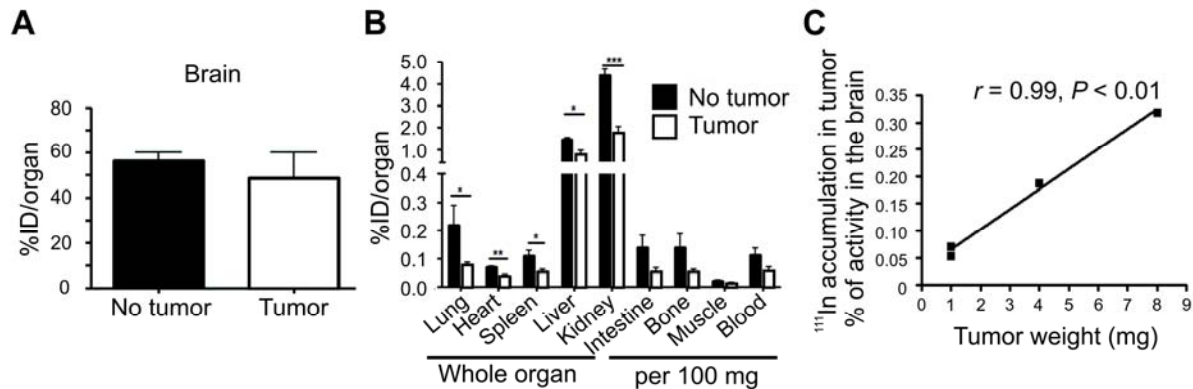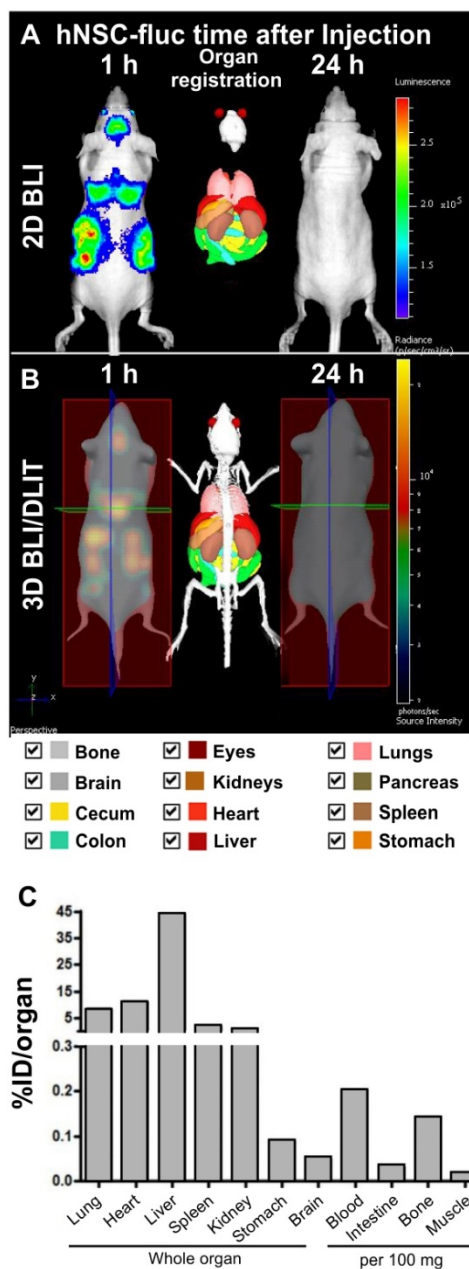
Supplemental Figure 4. Biodistribution study for intracranial injection of radiolabeled NSCs. A. [111]In activity in the mouse brain of control and tumor-bearing animals 48 hours after intracranial injection of NSCs loaded with ^{111}In-MSN. B. Distribution of ^{111}In by organ. C. Correlation study between tumor size and ^{111}In uptake.

Biodistribution study

In order to further test *in vivo* stability of our ^{111}In-MSN-based imaging system, the biodistribution study was carried out in the control and tumor-bearing animals. NSCs with ^{111}In radiolabeled MSN (2.0~2.5 MBq) were inoculated in the left hemispheres of brain (n=4 for each group) and animals were sacrificed 48 hours later. The brain and other tissues were taken out, weighed, and counted in a γ-counter calibrated for ^{111}In energy (Supplemental Fig. 4A,B). Supplemental Fig. 4A shows that the most ^{111}In activity was retained in the brain and it was similar between the control and tumor-bearing animals, indicating a similar persistence of radiolabeled NSCs in the brains of two groups of animals. Only a small fraction of radiolabel was found in the tumor tissue itself at indicated time point and the accumulation of radiotracer correlated well with the tumor size (Supplemental Fig. 4C). This is in agreement with our histological observations that most of the cells were localized in the peritumoral area rather than in the tumor mass itself at 48 hours after injection. The study of tissue biodistribution revealed

only low ^{111}In count present in each organ (in the range of 0.04-0.2% of total injected dose with an exception of the kidney (1.8-4.4%) and liver (0.8-1.5%) suggesting the hepatobiliary and renal routes of excretion of free radiotracer at this time point (Supplemental Fig. 4B). In conclusion, this data indicates that our NSCs loaded with ^{111}In-MSN represent a stable system suitable for studies investigating migration patterns towards malignancies and the fate of NSCs in the brain using SPECT imaging backed by microscopy data.

Supplemental Figure 5. Biodistribution of NSCs in mice after systemic injection. Biodistribution of NSC-fluc in mice was monitored by 2D bioluminescent imaging (BLI) and 3D BLI/DLIT (Diffuse Light Imaging Tomography) at 1 (A) and 24 hours (B) after systemic injection using IVIS Spectrum system. Organ registration was performed to extrapolate the BLI data. Distribution of

radiolabeled material in the tissues of sacrificed animal was assessed in 24 hours (C) after injection using gamma counter. Data are presented as % of ID per organ. Live NSCs were detected in the brain, lungs, liver, spleen and colon 1 hour after injection. No signal corresponding to live NSCs was present in the animals at 24 and 48 hours (not shown) after injection. However, radiolabeled material was detected in the liver, lungs, heart, spleen, kidneys, and in trace amounts in other organs 24 hours after injection.

Although biodistribution of NSCs after systemic injection is not under the scope of current study, our analysis revealed the presence of NSCs in major organs including brain at 1hour but not 24 hours after injection, indicating low engraftment and fast destruction of majority of injected NSCs via this route (Supplemental Fig. 5A and B), which is in agreement with previously published data (*7*). Since radiolabeled MSN are expected to release from NSCs upon their death *in vivo*, we measured radioactivity in tissue 24 hours after systemic injection (Supplemental Fig. 5C). In corroboration with the previous reports(*8-10*) our data show that the majority of radiolabeled MSN were present in the liver (about 44%), but also could be found in the lung (8%), heart (11%), spleen (2%) and kidney (1%) indicating release of ^{111}In-MSN from NSCs at sites of their initial accumulation. Small amount of radioactivity (0.1% and below) was detected in the blood and other assayed organs, thus further confirming the *in vivo* stability of ^{111}In-MSN complex. The biodistribution and safety profiles of MSN have been previously addressed in several publications (*8-10*) and, therefore, were not investigated in the current study.
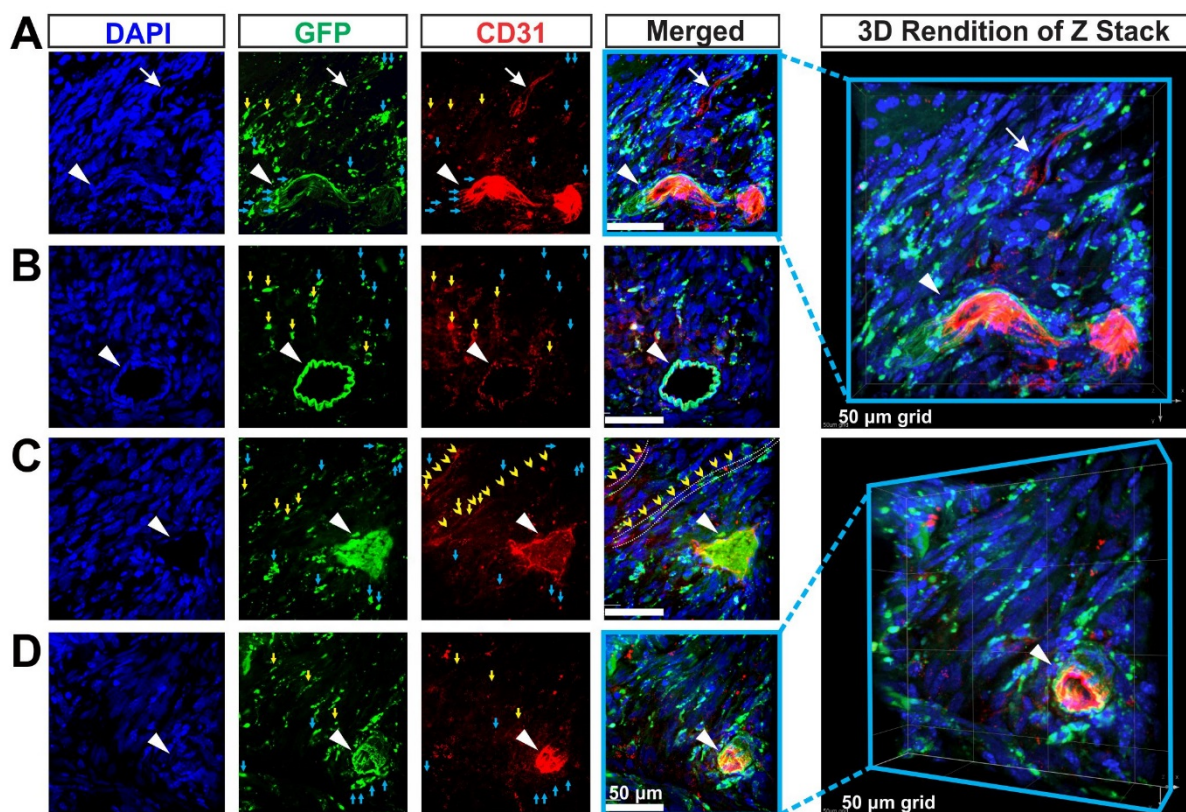
Supplemental Figure 6. Analysis of intratumoral distribution of systemically delivered NSCs. Staining and analysis of tissue sections for CD31, the vasculature endothelial marker (red), and GFP-positive NSCs, revealed that vast majority of NSCs are homed in to the U87 tumor mass or surrounding areas 48 hours after systemic injection. (A) A region where major blood vessel branch (white arrowhead) and small capillaries (white arrow) are seen together in the visual field. There are distinct signs of both, intra-vascular migrating NSCs (yellow arrows), which are spindle-shaped and strongly co-op with CD31-positive micro vessels, and extravasated NSCs (blue arrows) that are present in the parenchyma without any CD31-positive micro vessels in the vicinity. A 3D rendition of the confocal z-stack with 0.34 μm stack spacing shows clear and distinct CD31-reactivity of the interior surface of blood vessels, and the presence of GFP-positive NSCs on the outer surface of blood vessels adhering to the auto-fluorescent blood

vessel basement membrane (pale green sheath). (B) A cross section of a blood vessel within tumor bed demonstrates similar composite distributions of both intra-vessel GFP-positive NSCs (yellow arrows) and NSCs (blue arrows) extravasated into the surrounding tissue. Blood vessel shows strong auto-fluorescent of basement membrane (green ribbon) and CD31-immunoreactivity of the inner surface (red). (C) Occasional observation of micro blood vessels with GFP-positive NSCs inside can be made (white arrowhead). Both intra-vessel traveling GFP-positive NSCs (yellow arrows) along the traversing micro vessels (tangential sections outlined by white dotted lines and yellow arrowheads), as well as extravasated intra-parenchymal GFP-positive NSCs can be seen in the surrounding areas. (D) shows preferential accumulation of NSCs in the tumor mass outside of blood vessel.

SUPPLEMENTAL METHODS:

1. MSN Characterization

TEM images of MSN were obtained on a FEI Tecnai F30 microscope operated at an accelerating voltage of 120 kV. Standard TEM samples were prepared by dropping dilute products onto carbon-coated copper grids. Nitrogen adsorption-desorption isotherms were measured at 77 K using a Micromeritics ASAP 2020 system. The samples were pretreated under a vacuum at 393 K for 12 hours. Surface areas were determined using the BET method. Pore size distribution data were collected by the BJH method of the desorption branch of the isotherm. Dynamic light scattering (DLS) and zeta potential analysis were performed on a Nano-Zetasizer (Malvern Instruments Ltd.). Fluorescence spectra of decayed ^{111}In-MSN were analyzed using Marianas Yokogawa-type spinning disk confocal microscope (Photometrics, Tucson, AZ). Confocal fluorescent images of NSCs loaded with decayed ^{111}In-MSN were obtained using five separate color channels, excited by lasers with 405nm (blue), 445nm (cyan), 488nm (green), 561nm (red), 640nm (far red) wavelength. NSCs were visualized by staining

with anti-nestin polyclonal PE conjugated antibodies (BD Biosciences, San Jose, CA). In addition, the fluorescent spectra of active and decayed ^{111}In-MSN complex, as well as free ^{111}In were measured using HORIBA Fluorolog-3 Spectrofluorometer (HORIBA Jobin Yvon, Inc.). All samples were excited at 350 nm with 14 mm slit. All measurements were performed at room temperature in water.

2. Optimization of Labeling Efficiency and Stability Assessments

To optimize labeling efficiency, the conjugation was carried out at a molecular ratio of DOTA to MSN of 200, 500, 1000, 2000, 5000, and 10000 respectively. For radiolabeling of MSN, [111]In (37 MBq) was added to 1.6 mg of MSN-DOTA and incubated in the pH 5.5 MES buffer for 30 minutes, 1hr, 3hours, and 5hours. Radiolabeled MSN were purified by centrifugation and the labeling efficacy was measured by Instant Thin Layer Chromatography (ITLC) autoradiogram.

  For stability studies, ^{111}In-MSN-DOTA were incubated in serum free DMEM medium at 37 °C for up to 60 hours. Portions of the mixture were sampled at different time points and centrifuged for the detection of released isotope. The supernatants were collected and the radioactivity was measured. The retention of ^{111}In on the MSN-DOTA was calculated using the equation [(total radioactivity - radioactivity in filtrate)/total radioactivity] x 100%.

3. ICP-MS

  Quantification of silicon (Si) and cadmium (Cd) was accomplished using ICP-MS of acid digested samples. Specifically, 100 μL of BDH Aristar Plus Nitric Acid (70%, VWR Scientific, Radnor, PA, USA) was added to metal-free 15 mL conical tubes, followed by the addition of 10 μL of sample. Samples were then heated at 80 °C for 4 hours followed by addition of ultra-pure H_2O (18.2 MΩ·cm) and multi-element internal standard containing Bi, Ho, In,[6]Li, Sc, Tb, and Y (CLISS-1, Spex Certiprep, Metuchen, NJ, USA) to produce a final solution of 2% nitric acid (v/v) and 1 ng/g internal standard in a total sample volume of 3 ml.

  Individual Si and Cd elemental standards were prepared by diluting a 10.01 μg/mL of

certified Si and Cd standards (Inorganic Ventures, Christiansburg, VA, USA) to 488.44 ng/g and 99.243 Cd respectively. Si/Cd standards were then made via ½ serial dilution to obtain 9 elemental standards and a blank. All standards contained 2.0% nitric acid (v/v), and 1 ng/g internal standard up to a total sample volume of 5 ml.

ICP-MS was performed on a computer-controlled (QTEGRA software v. 2.4) Thermo iCapQc ICP-MS (Thermo Fisher Scientific, Waltham, MA, USA) operating in KED mode using He as a collision gas at 0.5 ml/min and equipped with a CETAC 260 autosampler (Omaha, NE, USA). Each sample was acquired using a 35 sec uptake and 90 sec washout time [rinse was 2.0% Aristar Plus HNO_3 (v/v)], 1 survey run (3 sweeps, 10 ms dwell time) and 3 main (peak jumping) runs (100 sweeps, 100 ms dwell time). The isotopes selected for analysis were ^{28}Si and ^{111,112,114}Cd, with ^{89}Y, ^{115}In, and ^{165}Ho chosen as internal standards for data interpolation. Instrument performance is optimized daily through autotuning followed by verification via a performance report (passing manufacturer specifications).

4. Uptake Efficiency, Cytotoxicity, and Phantom Study

In order to load NSCs with nanoparticles, 10^5 of NSCs were incubated ^{111}In- labeled MSN at 50, 100, and 200 µg/ml. Labeling was carried out in the DMEM medium containing 1% FBS or reduced serum Opti-MEM medium alone or in the presence of X-treme HP DNA transfection reagent (Roche Diagnostics, Indianapolis, IN) for 2 and 6 hours. After the incubation, NSCs were collected by trypsinization and centrifuged at 300g for 5 minutes. The supernatant and cell-associated radioactivity was measured in a gamma counter in order to calculate the uptake efficacy of radiolabeled nanoparticles in NSCs. The cytotoxicity of ^{111}In-MSN was evaluated using the standard luciferase assay protocol. NSCs expressing firefly luciferase (NSCs-fluc) were briefly incubated with ^{111}In-MSN at 25, 50, 100, and 200 µg/ml in Opti-MEM medium. In 2 hours, the medium was replaced with DMEM supplemented with 10% FBS; the cells were allowed to grow for 24 and 48 hours. At the end of incubation, the luciferase assay was carried

out according to manufacturer's instruction (Promega, Madison, WI). In order to determine the feasibility of SPECT imaging of NSCs loaded with ^{111}In-MSN, we carried out the *in vitro* phantom study, where ^{111}In-MSN loaded NSCs were injected at various amounts corresponding to 1.11, 0.56, 0.3 and 0 MBq and images were collected over 47 minutes.

5. SPECT Imaging Acquisition

The X-SPECT subsystem uses two CZT detectors with multiple pinhole apertures for each head, thereby increasing count sensitivity. Geometric corrections for pinhole size and alignment are combined with spiral acquisition to generate high-resolution images. Energy resolution is less than 5% at 140 keV. Animals were imaged with a 1-hour acquisition of tomographic data of 32 angels for the detection of NSCs loaded with ^{111}In labeled MSN (55-76 μCi) was performed at days 0, 1 and 2 post-injection.

6. Biodistribution

Mice were euthanized; brain and all major organs/tissues were collected and wet-weighed. The radioactivity in the tissue was measured using a gamma-counter (Perkin-Elmer, Waltham, MA) and presented as % of injected dose per organ. In order to estimate the tumor-associated radioactivity, xenograft tissue was separated from the brain parenchyma based on the expression of a cherry protein in U87MG cells, weighed, and analyzed for accumulated radioactivity. The biodistribution of NSCs-fluc was analyzed using 2D bioluminescent imaging (BLI) and 3D BLI/DLIT (Diffuse Light Imaging Tomography) at 1 and 24 hours after systemic injection. Distribution of radiolabeled material in the tissues of sacrificed animal was assessed at 24 hours as described above.

7. Tissue Processing and Histology

Tissue sections were prepared using a cryostat at a thickness of 10 μm. For detection of NSCs

loaded with ^{111}In-MSN, frozen sections were fixed in 4% paraformaldehyde and washed three times in PBS. Sections were then treated with 10% bovine serum albumin (BSA) 0.1% Triton X100 in PBS for 2 hours. The sections were then mounted in fluoromount-G medium supplemented with a nuclear stain DAPI. To confirm the location of the tumor, adjacent sections were stained with Hematoxylin & Eosin (H&E). The H&E staining was performed at The University of Chicago Human Tissue Resource Center according to the established protocol. Digital image files were created using a 3D Histech Pannoramic Scan whole slide scanner (Perkin Elmer, Waltham, MA) with a Zeiss AxioCam MRm CCD camera for fluorescent images (Carl Zeiss Microscopy, Thornwood, NY) or a Stingray F146C color camera for H&E sections (Allied Vision Technologies, Stadtroda, Germany). Individual images were created with the 3D Histech Pannoramic Viewer software (Perkin Elmer, Waltham, MA). Confocal microscopic images were captured with a 3i Marianas Yokogawa-type spinning disk confocal microscope with an Evolve EM-CCD camera (Photometrics, Tucson, AZ) running SlideBook v5.5 software (Intelligent Imaging Innovations, Denver, CO).

8.   **Characterization of intratumoral distribution of NSCs after systemic delivery.** In order to characterize the distribution and relationship between the systemically delivered GFP-positive NSCs and the intratumoral microvasculature, frozen tissue sections were processed as described above and endothelial cells of blood vessels were visualized using anti-CD31 antibody (rat IgG, dilution 1: 100; Santa Cruz Biotechnology, Santa Cruz, CA, USA) and AlexaFluor 647-conjugated secondary antibody (Jackson ImmunoResearch Inc., West Grove, PA, USA). After washing, the slides were mounted with Vectashield™ medium with DAPI (Vector Labs, Burlingame, CA, USA). Confocal images were captured and analyzed as described in the section above.

References

1.   ENSDF Decay Data for 111-In. *National Nuclear Data Center.* Retrieved 17 October 2012. http://www.orau.org/ptp/PTP%20Library/library/DOE/bnl/nuclidedata/MIRIn111.htm

2.   Bruchez M, Moronne M, Gin P, Weiss S, Alivisatos AP. Semiconductor Nanocrystals as Fluorescent Biological Labels. *Science.* 1998;281:2013-2016.

3.   Sooklal K, Hanus LH, Ploehn HJ, Murphy CJ. A Blue-Emitting CdS/Dendrimer Nanocomposite. *Adv Mater.* 1998;10:1083-1087.

4.   Balyasnikova IV, Prasol MS, Ferguson SD, et al. Intranasal delivery of mesenchymal stem cells significantly extends survival of irradiated mice with experimental brain tumors. *Mol Ther.* 2014;22:140-148.

5.   Ahmed AU, Thaci B, Alexiades NG, et al. Neural stem cell-based cell carriers enhance therapeutic efficacy of an oncolytic adenovirus in an orthotopic mouse model of human glioblastoma. *Mol Ther.* 2011;19:1714-1726.

6.   Ahmed AU, Thaci B, Tobias AL, et al. A preclinical evaluation of neural stem cell-based cell carrier for targeted antiglioma oncolytic virotherapy. *J Natl Cancer Inst.* 2013;105:968-977.

7.   Aboody KS, Najbauer J, Metz MZ, et al. Neural stem cell-mediumted enzyme/prodrug therapy for glioma: preclinical studies. *Sci Transl Med.* 2013;5:184ra159.

8.   He Q, Zhang Z, Gao F, Li Y, Shi J. In vivo biodistribution and urinary excretion of

mesoporous silica nanoparticles: effects of particle size and PEGylation. *Small.* 2011;7:271-280.

9. Lee CH, Cheng SH, Wang YJ, et al. Near-Infrared Mesoporous Silica Nanoparticles for Optical Imaging: Characterization and In Vivo Biodistribution. *Adv Funct Mater.* 2009;19:215-222.

10. Lu J, Liong M, Li Z, Zink JI, Tamanoi F. Biocompatibility, Biodistribution, and Drug-Delivery Efficiency of Mesoporous Silica Nanoparticles for Cancer Therapy in Animals. *Small.* 2010;6:1794-1805.